

## Identification of the first highly subtype-selective inhibitor of the human GABA transporter GAT3.

Maria Damgaard, Anas Al-Khawaja, Stine B Vogensen, Andreas Jurik, Maarten Sijm, Maria E.K. Lie, Mathias I Bæk, Emil Rosentahl, Anders A Jensen, Gerhard F. Ecker, Bente Frølund, Petrine Wellendorph, and Rasmus P. Clausen

ACS Chem. Neurosci., **Just Accepted Manuscript** • DOI: 10.1021/acscchemneuro.5b00150 • Publication Date (Web): 08 Jul 2015

Downloaded from <http://pubs.acs.org> on July 10, 2015

### Just Accepted

"Just Accepted" manuscripts have been peer-reviewed and accepted for publication. They are posted online prior to technical editing, formatting for publication and author proofing. The American Chemical Society provides "Just Accepted" as a free service to the research community to expedite the dissemination of scientific material as soon as possible after acceptance. "Just Accepted" manuscripts appear in full in PDF format accompanied by an HTML abstract. "Just Accepted" manuscripts have been fully peer reviewed, but should not be considered the official version of record. They are accessible to all readers and citable by the Digital Object Identifier (DOI®). "Just Accepted" is an optional service offered to authors. Therefore, the "Just Accepted" Web site may not include all articles that will be published in the journal. After a manuscript is technically edited and formatted, it will be removed from the "Just Accepted" Web site and published as an ASAP article. Note that technical editing may introduce minor changes to the manuscript text and/or graphics which could affect content, and all legal disclaimers and ethical guidelines that apply to the journal pertain. ACS cannot be held responsible for errors or consequences arising from the use of information contained in these "Just Accepted" manuscripts.



# Identification of the first highly subtype-selective inhibitor of the human GABA transporter GAT3.

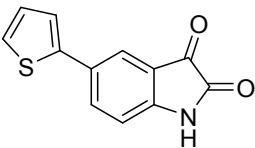
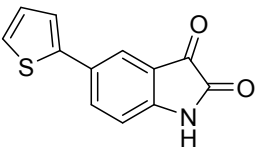
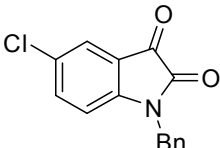
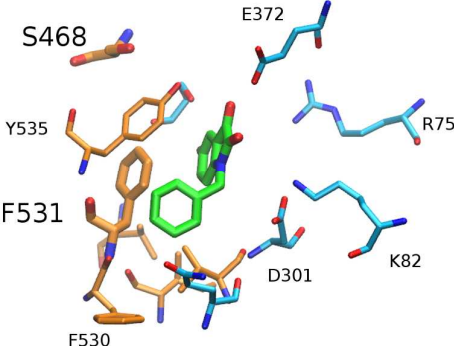
Maria Damgaard, Anas Al-Khawaja, Stine B. Vogensen, Andreas Jurik,<sup>#</sup> Maarten Sijm, Maria E.K. Lie, Mathias I. Bæk, Emil Rosenthal, Anders A. Jensen, Gerhard F. Ecker,<sup>#</sup> Bente Frølund, Petrine Wellendorph\* and Rasmus P. Clausen\*

Department of Drug Design and Pharmacology, Faculty of Health and Medical Sciences, University of Copenhagen, Universitetsparken 2, DK 2100 Copenhagen

<sup>#</sup>Department of Pharmaceutical Chemistry, University of Vienna, Althanstrasse 14, A-1090 Vienna, Austria.

\*Corresponding authors: Rasmus P. Clausen, Phone: +45 35 33 65 66, E-mail: rac@sund.ku.dk, Pharmacology: Petrine Wellendorph, Phone: +45 39 17 98 11, E-mail: pw@sund.ku.dk.

## Graphical table of contents

				
	(S)-SNAP-5114	<b>20</b>	<b>34</b>	
hGAT1:	>600 μM	>1000 μM	>1000 μM	
hBGT1:	405 μM	749 μM	>1000 μM	
hGAT2:	158 μM	203 μM	>1000 μM	
hGAT3:	45 μM	6 μM	29 μM	

## Abstract

Screening of a library of small-molecule compounds at a cell line expressing the human GABA transporter 3 (hGAT3) in a [<sup>3</sup>H]GABA uptake assay, identified isatin derivatives as a new class of hGAT3 inhibitors. A subsequent structure-activity relationship (SAR) study led to the identification of hGAT3 selective inhibitors (i.e. compounds **20** and **34**) that were superior to the reference hGAT3 inhibitor (S)-SNAP-5114 in terms of potency (low micromolar IC<sub>50</sub> values) and selectivity (>30 fold selective for hGAT3 over hGAT1/hGAT2/hBGT1). Further pharmacological characterization of compound **20** (5-(thiophen-2-yl)indoline-2,3-dione) revealed a non-competitive mode of inhibition at hGAT3. This suggests that the compound class, which has no structural resemblance to GABA, has a binding site different from the substrate GABA. This was supported by a molecular modeling study suggesting a unique binding site matching the observed selectivity, inhibition kinetics and SAR of the

compound series. These compounds are the most potent GAT3 inhibitors reported yet that provides selectivity for GAT3 over the other GABA transporter subtypes.

**Keywords:** GABA uptake, inhibitor, hGAT3 selective, non-competitive, kinetics, isatin

## Introduction

The major inhibitory neurotransmitter in the central nervous system,  $\gamma$ -aminobutyric acid (GABA) (**1**, Figure 1), plays a central role in normal brain function, and it has been demonstrated that abnormalities in GABAergic neurotransmission in the brain can lead to several disorders. Proteins involved in GABA neurotransmission are therefore interesting therapeutic targets and compounds perturbing this system in a selective manner are considered drug candidates for a number of diseases.<sup>1</sup> For example, epileptic and sleep disorders are treated with compounds acting at the GABAergic system, mainly by increasing GABAergic neurotransmission. An important part of the GABAergic system is the uptake of GABA into neurons and glial cells mediated by GABA transporters (GATs), and inhibition of this transport has been shown to be effective in the treatment of seizures in epileptic disorders.<sup>2</sup> The therapeutic relevance has been demonstrated by the GABA uptake inhibitor tiagabine (Gabitril<sup>TM</sup>) (**2**) that is a clinically approved drug used as add-on therapy for partial epilepsy.

Four different mammalian GABA transporters have been cloned, named GAT1, GAT2, GAT3 and BGT1 according to the IUPHAR nomenclature. GAT1 is the most studied transporter due to the existence of highly potent and specific inhibitors, such as tiagabine (**2**).<sup>3</sup> Development of highly selective compounds towards the other GABA transporters has been limited. GAT1 and GAT3 are exclusively present in the brain, but with a heterogenous distribution to primarily neurons (GAT1) and astrocytes (GAT3).<sup>4</sup> By contrast, BGT1 and GAT2 are also expressed in other organs, and although their expression levels in the brain are debated,<sup>5,6</sup> the role of BGT1 in relation to GABAergic neurotransmission is supported by the anticonvulsant effect of the mixed GAT1/BGT1 inhibitor (*RS*)-4-[*N*-[1,1-bis(3-methyl-2-thienyl)but-1-en-4-yl]-*N*-methylamino]-4,5,6,7-tetrahydrobenzo[*d*]isoxazol-3-ol (EF1502, **3**),<sup>7</sup> and a proposed role of BGT1 in regulating extrasynaptic GABA neurotransmission.<sup>8</sup> Much still remains to be learned about these transporter subtypes, but this requires more selective compounds.

Due to its exclusive expression in the brain and primary localization to astrocytes, GAT3 is a very interesting subtype and of potential clinical relevance in epilepsy and stroke,<sup>4,9</sup> but a role in neurons has also been demonstrated in some studies.<sup>10,11</sup> Although (*S*)-SNAP-5114 (**4**) is often applied as a “selective”

GAT3 inhibitor, the selectivity of the compound, and of several synthesized analogues<sup>12</sup> is not sufficiently pronounced to exclude effects on other GABA transporter subtypes. In addition, (*S*)-SNAP-5114 has a limited brain uptake and a modest chemical stability, thus limiting its use *in vivo*.<sup>13</sup> Consequently, there is a need to develop more selective GAT3 inhibitors that can be used to probe the physiological roles and therapeutic potential of this transporter.

The GABA transporters belong to the superfamily 6 of solute carriers (SLC6) that are Na<sup>+</sup>/Cl<sup>-</sup> dependent neurotransmitter transporters and share a common topology of 12 transmembrane (TM) spanning segments. Biochemical and X-ray crystallographic studies of members of this transporter family have provided knowledge on the transport mechanism. Currently, GABA is believed to be transported according to an alternate access model of substrate translocation, where GABA and co-transported ions are assumed to enter a central binding site from the extracellular space in an outward-open state of the transporter, followed by transition to a state, where GABA is occluded. Subsequently, an inward-facing conformation of the protein arises, with lower substrate affinity that triggers the release of the substrate into the cell.<sup>14</sup> Although still debated, it has been proposed that a secondary substrate binding site (S2) exists at the extracellular part of the occluded state that needs to be occupied to induce transport.<sup>15,16</sup> Currently, most of the known inhibitors of the GABA reuptake system display competitive inhibition at the central substrate binding site, but compounds with non-competitive profile have also been described.<sup>17</sup> Biostructural studies has enabled comparison of aligned GAT homology models, based on the crystal structures of the homologous bacterial leucine transporter LeuT and the *Drosophila melanogaster* dopamine transporter (DAT),<sup>18,19</sup> which offers the possibility of investigating potential subtype-selective binding cavities. Combined knowledge about steric demands of the inhibitor molecules and sequence differences facilitate docking studies for the generation of binding hypotheses.

In the current study we report the development of a new structural class of highly subtype-selective hGAT3 inhibitors that work in a non-competitive manner, possibly by acting at a new binding pocket for inhibition of the GABA transporters.

## Results and Discussion

A commercial compound library consisting of 4,000 structurally diverse compounds (Enamine, Monmouth, NJ, USA) was screened for their ability to inhibit the uptake of 30 nM [<sup>3</sup>H]GABA into Chinese Hamster Ovary (CHO) cells stably expressing the human GAT3 (hGAT3) subtype.<sup>20</sup> The bromo-/fluoro-substituted isatin **5** (Table 1) was identified as an hGAT3 inhibitor, thus representing a new structural scaffold among GABA uptake inhibitors bearing no structural resemblance to GABA. An extended characterization of commercially available analogues of **5** was performed as an initial structure-

activity relationship (SAR) study. 48 commercially available isatin analogues were tested in the [ $^3\text{H}$ ]GABA uptake assay at the hGAT3-CHO cell line in a single concentration. The structures of the 48 analogues and the results from this follow-up screening are presented in sFig. 1 in the Supporting Information. From this screening, nine compounds (**6-14**, Table 1) showed inhibition to a greater degree than the original hit (**5**) at hGAT3 and were consequently selected for further characterization at CHO cell lines expressing each of the four human GAT subtypes: hGAT1, hBGT1, hGAT2 and hGAT3. Concentration-inhibition curves were generated for each of the compounds, and the estimated  $\text{IC}_{50}$  values are presented in Table 1. The initial screening hit (**5**) displayed an inhibitory potency for hGAT3 of 108  $\mu\text{M}$  and an hGAT3/1 selectivity ratio of 5, however it did not discriminate between hBGT1, hGAT2 and hGAT3. Compounds with a small lipophilic substituent in the  $\text{R}_3$  position (**6**, **10** and **13**) displayed both higher hGAT3 potency and hGAT3/1 selectivity, whereas compounds lacking a substituent in the  $\text{R}_3$  position were weaker inhibitors at hGAT3. Moving the halogen to position  $\text{R}_2$ ,  $\text{R}_4$  and  $\text{R}_5$  completely abolished hGAT3 inhibition. The *N*-methylated compound (**11**) did not display more potent inhibition than the original hit, while the *N*-chloro compound (**12**) both improved hGAT3 potency and hGAT3/1 selectivity. Thus, activities of this scaffold responded well to the changes in substituents, and there seemed to be room for improvement of both hGAT3 potency and hGAT3/1 selectivity. Based on these findings, a series of compounds with different  $\text{R}_1$  and  $\text{R}_3$  substituents were designed to investigate critical areas for GAT3 inhibition and selectivity further. In particular, we wanted to explore how larger substituents in the  $\text{R}_3$  position and on the ring nitrogen would affect the GAT3 selectivity observed in the initial SAR.

The procedures for the synthesis of compounds **15-39** are depicted in scheme 1. The 5-alkyl substituted analogues **15** and **16** were synthesized via the Sandmeyer isonitrosoacetanilide isatin synthesis as previously described.<sup>21</sup> The reaction was not applicable for the 5-aryl substituted analogues. Instead, these analogues were synthesized via the Suzuki cross-coupling reaction.<sup>22</sup> Conditions previously described for Suzuki reactions on iodoisatins were tested.<sup>23,24</sup> However, low yields were obtained when coupling the 5-iodo or 5-bromoisatin under the described conditions. This has previously been described in cross coupling reactions of isatins.<sup>23</sup> Ketal protection of the free carbonyl group was tried to optimize the yields.<sup>23</sup> 5-Iodoisatin (**13**) and 5-bromoisatin (**40**) were refluxed with ethylene glycol and catalytic amounts of *p*-toluenesulfonic acid in toluene to yield the ketal-protected compounds **41** and **42**. The ketal-protected isatins **41** and **42** were cross-coupled with phenylboronic acid and (4-methoxyphenyl)boronic acid using the previously reported conditions<sup>25</sup> affording **43** and **44**. Deprotection of the ketal moiety in concentrated aqueous hydrochloric acid gave the desired compounds **17** and **23**, however in low yields. The overall yield of the Suzuki reactions did not differ substantially between the protected and

unprotected isatins, hence the unprotected reaction was preferred. A number of 5-aryl substituted analogues were synthesized using 5-iodoisatin directly in Suzuki cross-coupling reactions giving compounds **19-28**. *N*-alkylated analogues **29-39** were obtained using the alkyl halide and potassium carbonate in DMF under microwave-heating in fair yields.

All synthesized analogues were assayed at all four hGAT subtypes in the [<sup>3</sup>H]GABA uptake assay, and the results are presented in Table 2. Substitution of the isatin scaffold in the R<sub>3</sub> position with small aliphatic substituents (**15** and **16**) yielded IC<sub>50</sub> values of 49 and 15 μM at hGAT3 and an hGAT3/1 selectivity of 11 and 16, respectively. Increasing the size of the substituents in this position to larger aromatic substituents (**17**, **19-23**) increased the inhibitory potency at hGAT3 further, as these analogues exhibited IC<sub>50</sub> values in the low micromolar range and higher hGAT3/1 selectivity ratios (>29 or higher). In contrast, substitution of the distal aryl with groups larger than a methyl (**18**, **24-28**) led to complete loss of activity. For the *N*-substituted compounds, small substituents in the R<sub>1</sub> position (**29-30**) impaired potency for hGAT3, however potency was regained for larger substituents (**31-33**) and the R<sub>1</sub> benzyl-substituted compound **34** displayed an hGAT3 IC<sub>50</sub> value of 29 μM and an hGAT3/1 ratio greater than 100. Substitution on the R<sub>1</sub> benzyl group was detrimental to the activity of the compounds as the combination of an aryl group in the R<sub>3</sub> position and a benzyl in the R<sub>1</sub> position (**39**) completely abolished activity.

As can be seen from Tables 1 and 2, a number of the isatin analogues displayed partial inhibition of [<sup>3</sup>H]GABA uptake at their saturating concentrations. This phenomenon was seen in the concentration-inhibition curves as a bottom plateau less than the control value of 100% inhibition with 3 mM GABA. An example of such a curve is shown in figure 2A for **34** at hGAT3. For comparison, the concentration-inhibition curves for the isatin analogues **17** and **20** as well as the reference compound (*S*)-SNAP-5114 (**4**), which all displayed full uptake inhibition, are also included in Figure 2. Several of the isatin analogues (e.g. **34** at hGAT3, Figure 2A) displayed partial inhibition of [<sup>3</sup>H]GABA uptake with apparent plateaus ranging from 36% to 90% of control, a phenomenon reported previously for the dopamine transporter.<sup>26</sup> Whether the observed partial behavior of some isatin analogues is related merely to intrinsic pharmacological/structural properties of the compounds or to physicochemical properties, such as aggregation or reaching the solubility limits of the compounds at higher concentrations, is currently unclear. Clearly, solubility limits could mask either a full inhibition or a potential biphasic concentration-inhibition curve. The latter could exist if a compound binds with distinct affinities to two sites within the same transporter monomer, or with different affinities to two monomers of a transporter dimer. An example of biphasic uptake kinetics has been reported for the dopamine transporter,<sup>27</sup> and dimerization of GATs has been reported for the rat GAT1.<sup>28</sup>

Figure 2B highlights the pronounced hGAT3 over hGAT1 subtype-selectivity of compound **20** (more than 167 times), and that **20** is more potent than (*S*)-SNAP-5114 (**4**) (data summarized in Tables 1 and 2). In addition, compound **20** showed an hGAT3 selectivity of at least 30-fold over the other GAT subtypes while this is approximately 3 for (*S*)-SNAP-5114 (**4**). As described earlier, (*S*)-SNAP-5114 (**4**) has a limited use *in vivo* due to a limited brain uptake and a modest chemical stability.<sup>13</sup>

In addition to investigating the inhibitory activity of the synthesized compounds at the four hGATs, the mechanism underlying the inhibitions of GAT3 transport exerted by **20** was further investigated by measuring the transport rate of [<sup>3</sup>H]GABA in the absence and presence of different fixed concentrations of compound **20**. The results are shown in Figure 2C. Increasing the concentration of **20** resulted in a statistically significant decrease in  $V_{max}$ , while the  $pK_m$ -value was not significantly altered. This suggested that compound **20** inhibits the uptake of GABA through hGAT3 in a non-competitive manner. Kinetics studies were also performed for the structurally related compound **6**, showing the same kinetics profile and thereby confirming a non-competitive inhibition mode for the isatin analogues (results not shown). A non-competitive inhibition mode for these compounds is not surprising, since they show no structural resemblance with GABA.

A molecular modeling study was employed to suggest potential inhibitory binding sites for the compounds in the transporter that would be in accordance with the observed SAR and subtype-selectivity of the compounds. Cavity analysis of comparative models for all subtypes revealed a potential site in an outward-open state of GAT3 between TM domains 10 and 11, containing residues on positions 10.49 (S468) and 11.60 (F531) (generic numbering according to Beuming et al. 2006<sup>29</sup> see Figure 3 and alignment in sFig. 2 in the Supporting Information) that are not conserved in the three other human GATs. As it can be seen in Figure 3, substrates could still enter the central binding cavity, and also the disputed secondary substrate binding site S2 is accessible. Thus, a non-competitive mode of inhibition could root from impaired TM rearrangement needed for substrate translocation to the intracellular space.

Placement of the isatin derivatives into this site using a flexible docking workflow indicated a possible binding mode, which is in line with the SAR. For selected compounds, short molecular dynamics simulations in a membrane environment were performed for exploring solvent-mediated interactions with surrounding residues.

The hydrophobic side of the compounds was mainly accommodated in the hydrophobic part of the pocket. An aromatic residue in position 10.64, which is present in all subtypes except hGAT1, was observed to support hydrophobic interactions with aromatic substituents in the 1- or 5-position and supporting the selectivity trends of the dataset, as exemplified by compounds **17-23** and **34**. The position

of the polar oxo groups seem to be stabilized by a complex water-mediated hydrogen bond network, occasionally involving polar residues of TM1, 6 and the extracellular loop EL4. The fragile character of this network is underlined by inactivity of compounds **45** and **46**, being substituted at the position of the 3-oxo group.

As exemplified by hGAT1 and 3 in Figure 4, similar initial ligand placements could be observed for all four hGAT subtypes, but non-hGAT3 complexes were significantly less stable and displayed pronounced drifting of the ligands in the short molecular dynamics simulations. This underlines the importance of hydrophobic properties, as residues 10.49 (Y/Y/Y/S) and 11.60 (S/S/S/F) are, albeit switched, nearly identical for all of the GAT subtypes. Hence, the small difference of a phenolic hydroxyl group could cause the particular pharmacological properties of the data set.

Herein, we have reported the design, synthesis and pharmacological evaluation of a new type of hGAT3 selective inhibitors, based on the isatin scaffold. Compound **20** is a more potent analogue than the reference GAT3 inhibitor (*S*)-SNAP-5114 (**4**), and also the selectivity for hGAT3 compared to the other subtypes is significantly improved. Thus, selectivity for hGAT3 over hGAT2 and hBGT1 is increased from 3.5- and 9- fold to 34- and 124-fold, respectively. Some of the compounds display partial inhibition of the GABA transport. Interestingly, these compounds were shown to have a non-competitive inhibition mode at hGAT3, which together with the lack of structural resemblance to GABA suggests a different binding site to previous inhibitors. Many of the previous GABA uptake inhibitors bear an amino and acid group, suggesting a binding site partially overlapping with GABA. A molecular modeling study evaluated potential binding sites in a full range of GABA transporter homology models and only one binding site had the size and physiochemical characteristics that were in accordance with observed potency and selectivity trends, which awaits further experimental validation. This is part of future studies that will also be directed at determining the blood-brain barrier permeability of selected analogues. Also, studies on the effect of compound **20** at neurons and astrocytes under normal and diseased conditions, and how it could influence synaptic vesicle recycling, transporter exo/endocytosis are of high importance. In conclusion, we have presented a new class of hGAT3 selective compounds that can be used as tool compounds to understand the pharmacology of hGAT3 and its involvement in disease.

## Methods

## Chemistry

**General procedures.** All anhydrous reactions were carried out in oven-dried glassware, under nitrogen. Solvents were of chromatography grade and dried using an SG Water solvent purification



system (DCM, DMF, and THF) or with 3 Å molecular sieves. Commercially obtained chemicals were used without further purification. TLC was carried out on Merck precoated silica gel 60 F254 plates and visualized using UV (254 nm). Column purifications were carried out manually using silica gel: 40–63 µm. NMR spectra were recorded on a 400 MHz Bruker Avance or a 600 MHz Bruker Avance instrument. Data reported as follows: chemical shift, multiplicity (s = singlet, d = doublet, dd = double doublet, t = triplet, bs = broad singlet, m = multiplet), integration and coupling constants (Hz). Chemical shifts are reported in ppm with the solvent resonance resulting from incomplete deuteration as the internal reference (CHCl<sub>3</sub> in CDCl<sub>3</sub>: δ 7.26, (CH<sub>3</sub>)<sub>2</sub>SO in (CD<sub>3</sub>)<sub>2</sub>SO: δ 2.50), exception being samples in D<sub>2</sub>O, to which 40 µl of dioxane per 100 ml D<sub>2</sub>O was added as reference (dioxane in D<sub>2</sub>O: δ 3.75). A few NMR spectra have been attached in appendix T. Analytical HPLC was performed on a Merck-Hitachi HPLC system consisting of an L-7100 pump, an L-7200 auto sampler, and an L-7400 UV detector (254 nm), using an Chromolith SpeedROD RP-18 column (4.6 × 50 mm) eluted at a flow rate of 4.0 mL/min. A linear gradient elution was performed with eluent A (H<sub>2</sub>O/TFA 100:0.1) containing 0% of solvent B (MeCN/H<sub>2</sub>O/TFA, 90:10:0.01) rising to 100% of B during 5 min. Data were acquired and processed using the EZChrom Elite Software version 3.1.7 by Hitachi. HPLC purity is ≥ 95%, unless otherwise stated. LCMS method A: LC-MS was performed using a Agilent 1100 HPLC systems with a XBridge 3.5 µm C-18 column (100 × 4.60 mm) using gradient elution from buffer A (H<sub>2</sub>O:CH<sub>3</sub>CN:HCOOH, 95:5:0.1) to buffer B (H<sub>2</sub>O:CH<sub>3</sub>CN: HCOOH, 5:95:0.05) over 10 min flow rate: 1.0 mL/min, coupled to an Hewlett Packard 1100 series mass spectrometer with an electrospray ionization source.. LCMS method B: HPLC-MS was recorded on an Agilent 1200 series system using an Xbridge RP C18 column (3.5 µm, 100 × 4.6 mm) with UV detection at 210, 254 and 280 nm. Mobile phase (MP) A: 0.2% HCOOH, 99.8% H<sub>2</sub>O (v/v). Mobile phase B: 0.2% HCOOH, 99.8% MeCN (v/v). Flow rate: 1 ml/min. Gradient: 0-7 min: 0-90% MP B, 7-9 min: 90% MP B, 9-16 min: 10% MP B.

**5-(thiophen-2-yl)indoline-2,3-dione (20).** 5-iodoindoline-2,3-dione (**13**) (0.1 g, 0.36 mmol), thiophene-2-boronic acid pinacol ester (0.090 g, 0.43 mmol) and NaHCO<sub>3</sub> (0.06 g, 0.72 mmol) were dissolved in a mixture of DME:H<sub>2</sub>O (5:1, 4.8 mL). The mixture was degassed with N<sub>2</sub> gas, after which Pd(dppf)Cl<sub>2</sub> (15 mg, 0.018 mmol) was added and the reaction vial was sealed and heated at 90°C for 18 hour. The crude reaction mixture was filtered over Celite and diluted with EtOAc, after which the organic layer was washed with a saturated NaHCO<sub>3</sub> solution. Organic layer was dried over MgSO<sub>4</sub>, after which volatiles were evaporated under reduced pressure. The resulting crude solids were purified over SiO<sub>2</sub> using a gradient of 4:1 n-heptane:EtOAc towards 2:1 n-heptane:EtOAc yielding 10 mg of title compound (0.042 mmol, 12%). <sup>1</sup>H NMR (600 MHz, DMSO-*d*<sub>6</sub>) δ 11.14 (s, 1H), 7.86 (dd, *J* = 8.2, 2.0 Hz, 1H), 7.75 (d, *J* = 2.0 Hz, 1H), 7.55 – 7.51 (m, 1H), 7.15 – 7.11 (m, 1H), 6.96 (d, *J* = 8.2 Hz, 1H). <sup>13</sup>C NMR (101 MHz, DMSO-*d*<sub>6</sub>) δ 184.63, 159.91, 150.11, 142.43, 135.43, 129.19, 129.05, 125.88, 124.11, 121.46,

118.92, 113.25. LC-MS (ESI) m/z calculated for  $C_{12}H_8NO_2S^+$ : 230.26 found: 230.1  $[M+H]^+$ , retention time: 6.054 minutes.

### Materials, [ $^3H$ ]GABA uptake assay

Ham's F12 Nutrient Mix, fetal bovine serum (FBS), penicillin–streptomycin, hygromycin B, trypsin and Hank's Balanced Salt Solution (HBSS, catalogue number 14175-095) were purchased from Life Technologies (Paisley, UK). Plasmocin was obtained from InvivoGen (San Diego, CA, USA). Poly-D-lysine (PDL) and HEPES (4-(2-hydroxyethyl) piperazine-1-ethanesulfonic acid) were purchased from Sigma-Aldrich. [2,3- $^3H(N)$ ] GABA (specific radioactivity 35.0 Ci/mmol) and MicroScint-20 were purchased from PerkinElmer (Boston, MA, USA). GABA was purchased from Sigma-Aldrich (St. Louis, MO, USA). The isatin analogues **5-14** (see Table 1) were generously provided by 7TM Pharma, Denmark.

### Cell culture and GAT expression

Generation and culture of the Chinese hamster ovary (CHO) Flp-in cell line stably expressing the human GATs have been previously described.<sup>17,20</sup>

### [ $^3H$ ]GABA uptake assay and compound library screening

The [ $^3H$ ]GABA competition uptake assay and kinetics studies were performed exactly as previously described using a 96-well format setup.<sup>20</sup>

### Data analysis

Data and statistical analysis were performed in GraphPad Prism 6 (GraphPad Software, San Diego, CA, USA). Concentration-inhibition curves generated in the competition [ $^3H$ ]GABA uptake assay were fitted by nonlinear regression using the equation for sigmoidal concentration-response with variable slope:  $Y = \text{Bottom} + (\text{Top} - \text{Bottom}) / (1 + 10^{((\log IC_{50} - X) \times \text{HillSlope}))}$ , where Y is the response, X is the logarithm of the concentration, Top and Bottom are the plateaus in same units as Y, and  $\log IC_{50}$  is the concentration giving a response half way between Bottom and Top. The HillSlope is the steepness of the curve. Concentration-inhibition curves were fitted to 100% inhibition by 3 mM GABA if the highest

concentration of the inhibitor displayed less than 90% but more than 50% inhibition of [<sup>3</sup>H]GABA uptake. The IC<sub>50</sub> values of compounds displaying less than 50% but more than 10% inhibition were estimated as being greater than the highest tested concentration. Compounds showing less than 10% [<sup>3</sup>H]GABA uptake inhibition at the highest tested concentration were considered not active.

Data from kinetics experiments were analyzed using the Michaelis-Menten equation:  $Y = V_{\max} * X / (K_m + X)$ , where Y is the uptake velocity, X is substrate concentration,  $V_{\max}$  is the maximum uptake velocity in the same units as Y, and  $K_m$  is the Michaelis-Menten constant in the same unit as X.

### Molecular modeling

Models of hGAT1-3 and hBGT1 were constructed using Modeller 9.14, using inward-facing, outward-occluded-and outward-open template structure of LeuT (PDB codes 3TT3, 2A65, 3F3A). Initial sequence alignment according to Beuming et al.<sup>29</sup> was further optimized in loop regions (see Supporting Information sFig.2). Crystal structures of MhsT and DAT<sub>cryst</sub> were consulted for resolving secondary structural ambiguities. 200 models for each transporter in all three conformations were generated and sorted according to DOPE Score.

Site Finder module of MOE 2014.09 was used for cavity analysis. Docking studies were carried out using the Schrödinger 2014.3 Suite. Structure preparation was performed with LigPrep, docking with the Induced Fit Docking protocol. Isatin derivatives were drawn within MOE and prepared with LigPrep, sampled for a physiological pH range of 7.2 +/- 0.2.

MD simulations were performed for 10 ns using Desmond 3.6 and the OPLS 2005 force field, n=3 for hGAT1 and hGAT3. Protein models were placed in a POPC membrane manually adjusted after being set to TM residues, and solvated using an SPC water model and 0.15 M NaCl. Trajectory analysis was carried out using VMD and Desmond's Simulation Interaction Diagram.

### Supporting information

Synthetic procedures for the synthesis of for compound **15-39** can be found in the Supporting Information along with results and structures of the follow-up screening of 48 isatin analogues and molecular modeling data. This material is available free of charge via the Internet at <http://pubs.acs.org>.

### Abbreviations.

BGT1, betaine-GABA transporter; CHO, chinese hamster ovary; CNS, central nervous system; GABA,  $\gamma$ -aminobutyric acid; GAT, GABA transporter; SAR, structure-activity relationship; (S)-SNAP 5114, 1-[2-[*tris*(4-methoxyphenyl)methoxy]ethyl]-(S)-3-piperidinecarboxylic acid; TM, transmembrane.

**Author Information.**

Current address: Department of Drug Design and Pharmacology, Faculty of Health and Medical Sciences, University of Copenhagen, Universitetsparken 2, DK 2100 Copenhagen

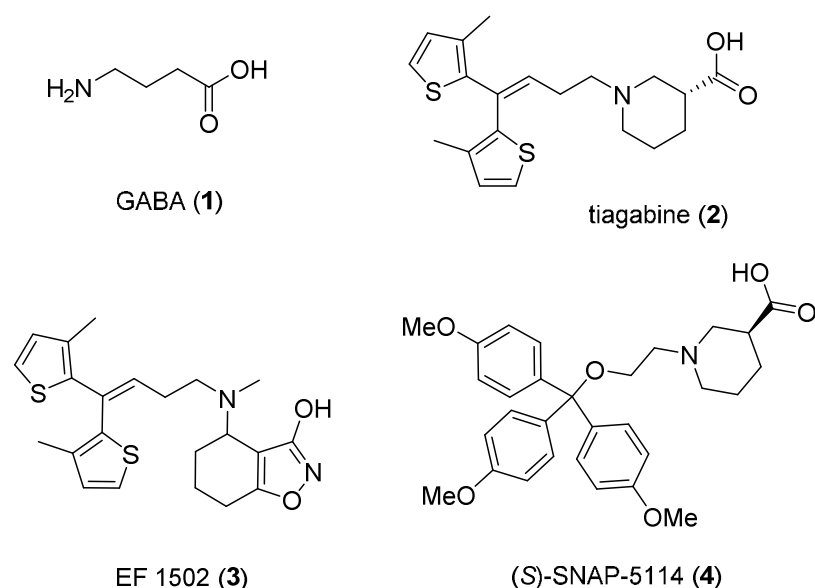
Funding: This work was supported by the Lundbeck Foundation, the Novo Nordisk Foundation, the A.P. Møller Foundation for the Advancement of Medical Sciences, and the Drug Research Academy.

The authors declare no competing financial interest.

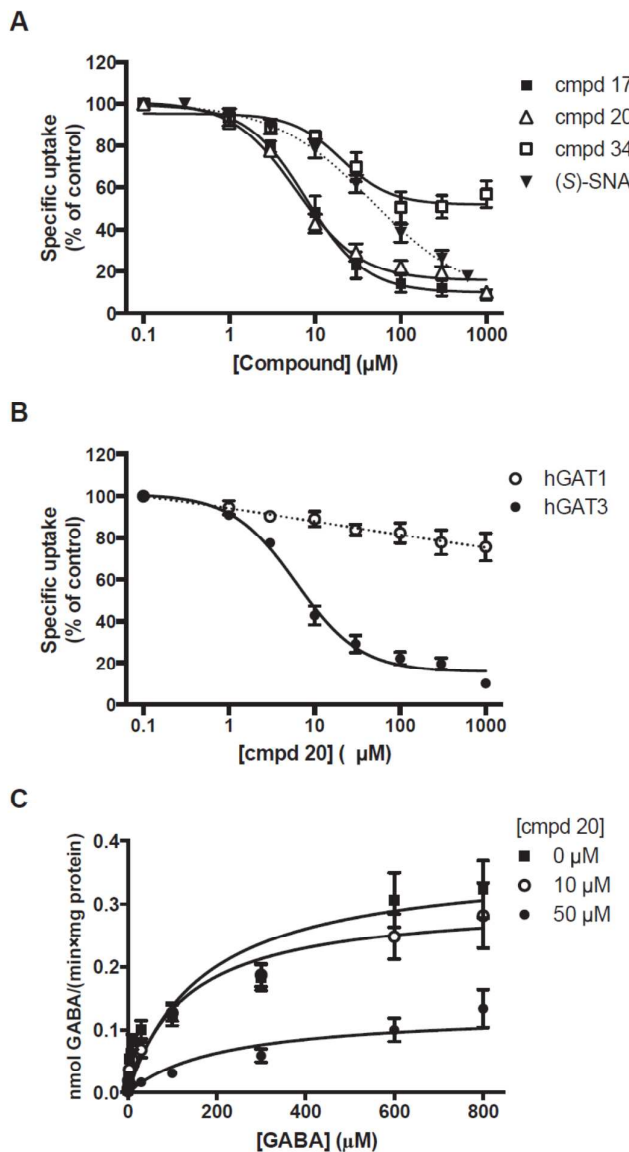
## References.

1. Rowley, N. M., Madsen, K. K., Schousboe, A., and Steve White, H. (2012) Glutamate and GABA synthesis, release, transport and metabolism as targets for seizure control, *Neurochem. Int.* 61, 546-558.
2. Meldrum, B. S., and Chapman, A. G. (1999) Basic Mechanisms of Gabitril (Tiagabine) and Future Potential Developments, *Epilepsia* 40, S2-S6.
3. Nielsen, E. B., Suzdak, P. D., Andersen, K. E., Knutsen, L. J., Sonnewald, U., and Braestrup, C. (1991) Characterization of tiagabine (NO-328), a new potent and selective GABA uptake inhibitor, *Eur.J. Pharmacol.* 196, 257-266.
4. Madsen, K. K., White, H. S., and Schousboe, A. (2010) Neuronal and non-neuronal GABA transporters as targets for antiepileptic drugs, *Pharmacol. Therapeut* 125, 394-401.
5. Borden, L. A. (1996) GABA transporter heterogeneity: pharmacology and cellular localization, *Neurochem. Int.* 29, 335-356.
6. Lehre, A. C., Rowley, N. M., Zhou, Y., Holmseth, S., Guo, C., Holen, T., Hua, R., Laake, P., Olofsson, A. M., Poblete-Naredo, I., Rusakov, D. A., Madsen, K. K., Clausen, R. P., Schousboe, A., White, H. S., and Danbolt, N. C. (2011) Deletion of the betaine-GABA transporter (BGT1; slc6a12) gene does not affect seizure thresholds of adult mice, *Epilepsy Res.* 95, 70-81.
7. White, H. S., Watson, W. P., Hansen, S. L., Slough, S., Perregaard, J., Sarup, A., Bolvig, T., Petersen, G., Larsson, O. M., Clausen, R. P., Frolund, B., Falch, E., Krogsgaard-Larsen, P., and Schousboe, A. (2005) First demonstration of a functional role for central nervous system betaine/{gamma}-aminobutyric acid transporter (mGAT2) based on synergistic anticonvulsant action among inhibitors of mGAT1 and mGAT2, *J. Pharmacol. Exp. Therapeut.* 312, 866-874.
8. Madsen, K. K., Ebert, B., Clausen, R. P., Krogsgaard-Larsen, P., Schousboe, A., and White, H. S. (2011) Selective GABA transporter inhibitors tiagabine and EF1502 exhibit mechanistic differences in their ability to modulate the ataxia and anticonvulsant action of the extrasynaptic GABA(A) receptor agonist gaboxadol, *J. Pharmacol. Exp. Therapeut.* 338, 214-219.
9. Clarkson, A. N., Huang, B. S., Macisaac, S. E., Mody, I., and Carmichael, S. T. (2010) Reducing excessive GABA-mediated tonic inhibition promotes functional recovery after stroke, *Nature* 468, 305-309.
10. Melone, M., Cozzi, A., Pellegrini-Giampietro, D.E. and Conti F. (2003) Transient focal ischemia triggers neuronal expression of GAT-3 in the rat perilesional cortex. *Neurobiol Dis.* 14, 120-132.
11. Pozdnyakova, N., Dudarenko, M., Yatsenko, L., Himmelreich, N., Krupko, O., and Borisova, T. (2014). Perinatal hypoxia: different effects of the inhibitors of GABA transporters GAT1 and GAT3 on the initial velocity of [<sup>3</sup>H]GABA uptake by cortical, hippocampal, and thalamic nerve terminals. *Croat. Med. J.* 55, 250-258.
12. Pabel, J., Faust, M., Prehn, C., Worlein, B., Allmendinger, L., Hofner, G., and Wanner, K. T. (2012) Development of an (S)-1-{2-[tris(4-methoxyphenyl)methoxy]ethyl}piperidine-3-carboxylic acid [(S)-SNAP-5114] carba analogue inhibitor for murine gamma-aminobutyric acid transporter type 4, *ChemMedChem* 7, 1245-1255.
13. Dalby, N. O. (2000) GABA-level increasing and anticonvulsant effects of three different GABA uptake inhibitors, *Neuropharmacol.* 39, 2399-2407.

14. Kristensen, A. S., Andersen, J., Jorgensen, T. N., Sorensen, L., Eriksen, J., Loland, C. J., Stromgaard, K., and Gether, U. (2011) SLC6 neurotransmitter transporters: structure, function, and regulation, *Pharmacol. Rev.* **63**, 585-640.
15. Reyes, N., and Tavoulari, S. (2011) To be, or not to be two sites: that is the question about LeuT substrate binding, *J. Gen. Physiol.* **138**, 467-471.
16. Quick, M., Shi, L., Zehnpfennig, B., Weinstein, H., and Javitch, J. A. (2012) Experimental conditions can obscure the second high-affinity site in LeuT, *Nat. Struct. Mol. Biol.* **19**, 207-211.
17. Kragholm, B., Kvist, T., Madsen, K. K., Jorgensen, L., Vogensen, S. B., Schousboe, A., Clausen, R. P., Jensen, A. A., and Brauner-Osborne, H. (2013) Discovery of a subtype selective inhibitor of the human betaine/GABA transporter 1 (BGT-1) with a non-competitive pharmacological profile, *Biochem. Pharmacol.* **86**, 521-528.
18. Yamashita, A., Singh, S. K., Kawate, T., Jin, Y., and Gouaux, E. (2005) Crystal structure of a bacterial homologue of Na<sup>+</sup>/Cl<sup>-</sup>-dependent neurotransmitter transporters, *Nature* **437**, 215-223.
19. Penmatsa, A., Wang, K. H., and Gouaux, E. (2013) X-ray structure of dopamine transporter elucidates antidepressant mechanism, *Nature* **503**, 85-90.
20. Al-Khawaja, A., Petersen, J. G., Damgaard, M., Jensen, M. H., Vogensen, S. B., Lie, M. E., Kragholm, B., Brauner-Osborne, H., Clausen, R. P., Frolund, B., and Wellendorph, P. (2014) Pharmacological identification of a guanidine-containing beta-alanine analogue with low micromolar potency and selectivity for the betaine/GABA transporter 1 (BGT1), *Neurochem. Res.* **39**, 1988-1996.
21. Sandmeyer, T. (1919) Über Isonitrosoacetanilide und deren Kondensation zu Isatinen, *Helv. Chim. Acta* **2**, 234-242.
22. Miyaura, N., and Suzuki, A. (1995) Palladium-Catalyzed Cross-Coupling Reactions of Organoboron Compounds, *Chem. Rev.* **95**, 2457-2483.
23. Gérard, A. L., Lisowski, V., and Rault, S. (2005) Direct synthesis of new arylanthranilic acids via a Suzuki cross-coupling reaction from iodoisatins, *Tetrahedron* **61**, 6082-6087.
24. Liu, Y. C., Ye, C. J., Chen, Q., and Yang, G. F. (2013) Efficient synthesis of bulky 4-substituted-isatins via microwave-promoted Suzuki cross-coupling reaction, *Tetrahedron Lett.* **54**, 949-955.
25. Wang, C. H., White, A. R., Schwartz, S. N., Alluri, S., Cattabiani, T. M., Zhang, L. K., Chan, T. M., Buevich, A. V., and Ganguly, A. K. (2012) Novel synthesis and functionalization of ortho-ortho disubstituted biphenyls and a highly condensed novel heterocycle using radical cyclization reaction, *Tetrahedron* **68**, 9750-9762.
26. Ananthan, S., Saini, S. K., Khare, R., Clayton, S. D., Dersch, C. M., and Rothman, R. B. (2002) Identification of a novel partial inhibitor of dopamine transporter among 4-substituted 2-phenylquinazolines, *Bioorg. Med. Chem. Lett.* **12**, 2225-2228.
27. Lee, F. J., Pristupa, Z. B., Ciliax, B. J., Levey, A. I., and Niznik, H. B. (1996) The dopamine transporter carboxyl-terminal tail. Truncation/substitution mutants selectively confer high affinity dopamine uptake while attenuating recognition of the ligand binding domain, *J. Biol. Chem.* **271**, 20885-20894.
28. Scholze, P., Freissmuth, M., and Sitte, H. H. (2002) Mutations within an intramembrane leucine heptad repeat disrupt oligomer formation of the rat GABA transporter 1, *J. Biol. Chem.* **277**, 43682-43690.
29. Beuming, T., Shi, L., Javitch, J. A., and Weinstein, H. (2006) A comprehensive structure-based alignment of prokaryotic and eukaryotic neurotransmitter/Na<sup>+</sup> symporters (NSS) aids in the use of the LeuT structure to probe NSS structure and function, *Mol. Pharmacol.* **70**, 1630-1642.



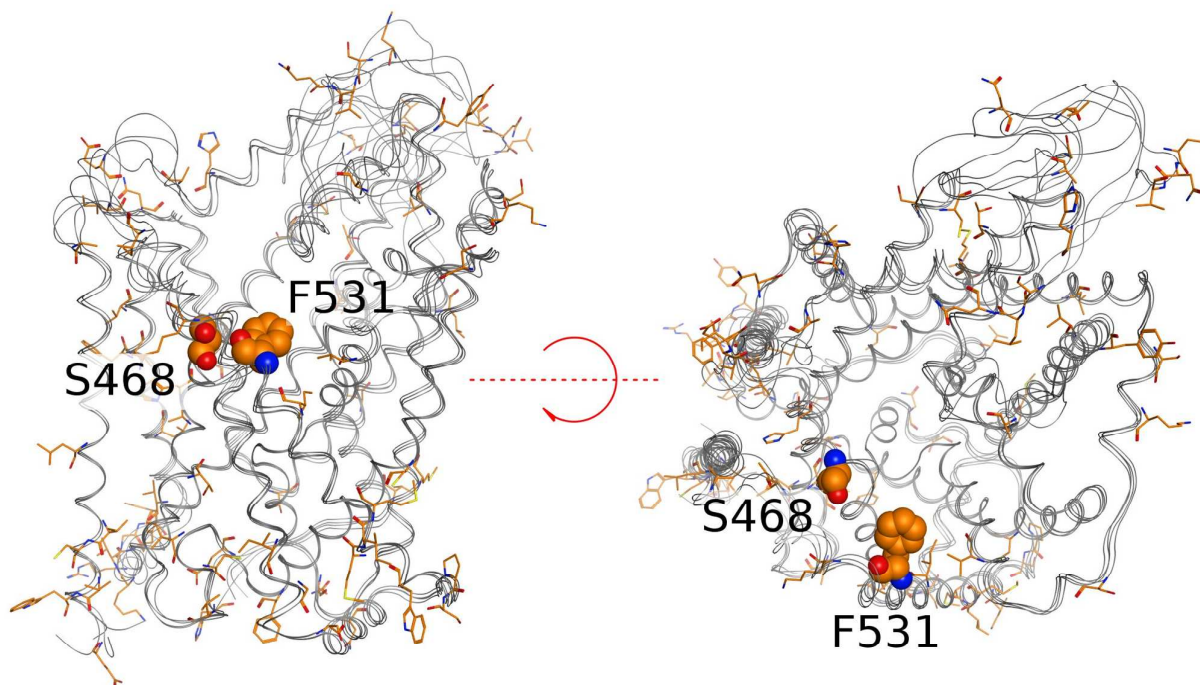
**Figure 1.** Structures of  $\gamma$ -aminobutyric acid (GABA, 1), the highly GAT1 selective inhibitor tiagabine (2), and EF 1502 (3), a mixed BGT1/GAT1 inhibitor and the moderately potent GAT3 inhibitor (S)-SNAP-5114 (4).



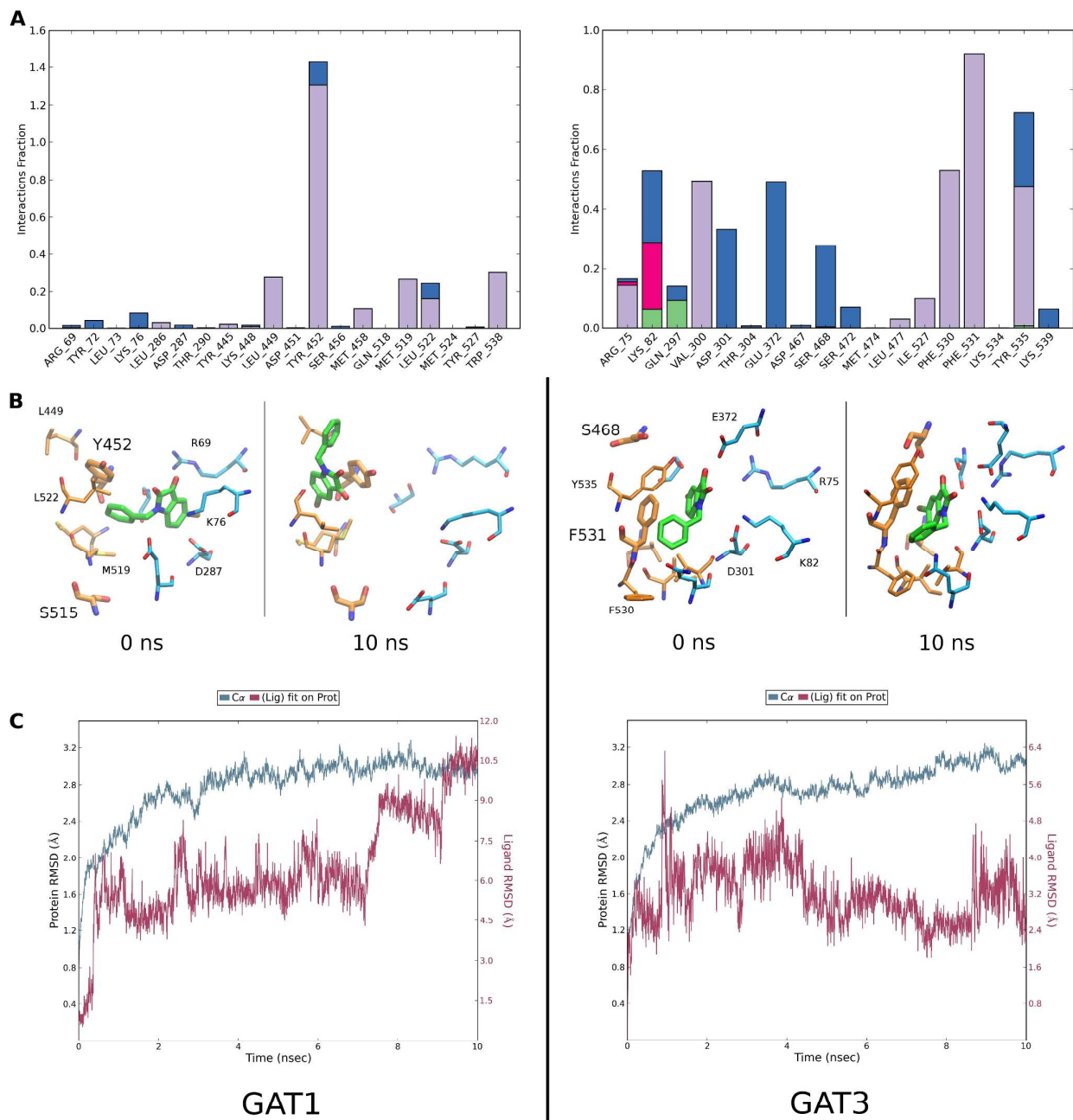
**Figure 2.** Pharmacological characterization of novel isatin analogues at hGATs, stably expressed in CHO cells. **(A)** Concentration-inhibition curves for **17**, **20**, **34** and (S)-SNAP-5114 (**4**) at hGAT3. **34** displayed partial inhibition of [<sup>3</sup>H]GABA uptake. The responses are normalized mean values of at least three independent experiments ± S.E.M. (see tables 1 and 2 for mean IC<sub>50</sub> values). **(B)** Concentration-inhibition curves for compound **20** at hGAT1 and hGAT3. The responses are normalized mean values of three independent experiments ± S.E.M. Estimated IC<sub>50</sub> value at hGAT1: >1000 μM; and at hGAT3: 6 μM (table 2). **(C)** Effect of compound **20** on the GABA transport velocity through hGAT3. Specific transport velocity of increasing concentrations of GABA was measured in the [<sup>3</sup>H]GABA uptake assay. The maximum concentration of [<sup>3</sup>H]GABA was 100 nM. Data are given as nmol GABA transported per minute and normalized to protein amount per well. Results are mean values of three independent experiments ± S.E.M. The  $K_m$  values expressed in μM ( $pK_m$  ± S.E.M.) were estimated to be: 0 μM **20**, 172 ( $3.77 \pm 0.03$ ); 10 μM **20**, 201 ( $3.82 \pm 0.24$ ); 50 μM **20**, 246 ( $3.65 \pm 0.13$ ). The  $V_{max}$  values expressed as nmol GABA/(min×mg protein) ± S.E.M. were estimated to be: 0 μM **20**,  $0.39 \pm 0.06$ ; 10 μM **20**,  $0.28 \pm 0.04$ ; 50 μM **20**,  $0.13 \pm 0.01$  (the  $V_{max}$  value was constrained to the average of the maximal level). The



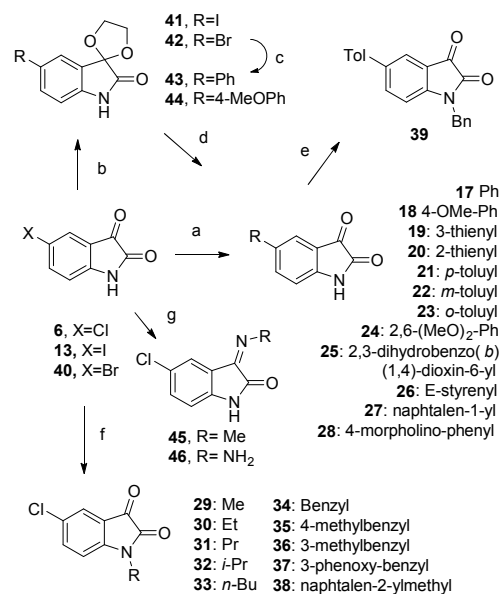
$V_{max}$  value in the presence of 50  $\mu\text{M}$  **20** was significantly decreased compared to control, but no significant different in  $pK_m$  was present (One-way ANOVA followed by Dunnett's test,  $P < 0.01$ ).



**Figure 3.** Localization of GAT3 selective residues (orange). Amino acids 10.49 (S468) and 11.60 (F531) located in the putative pocket depicted in Van der Waals surface.



**Figure 4.** Molecular dynamics behavior of **34** at hGAT1 and hGAT3. **A:** protein-ligand contacts over the trajectory. Hydrophobic contacts depicted in purple, hydrogen bonds in green, ionic in pink, water bridges in blue. **B:** ligand position relative to key residues at the beginning and the end of the simulation. **C:** protein (blue) and ligand (purple) root mean square of deviation (RMSD).

Scheme 1. Synthesis of 17-46<sup>a</sup>

<sup>a</sup>Reagents and conditions: (a) R-B(OH)<sub>2</sub>, Pd(dppf)Cl<sub>2</sub>, NaHCO<sub>3</sub>, DME, H<sub>2</sub>O, heating, 2-12%, (b) Ethylene glycol, PTSA (p-toluenesulfonic acid), Toluene, reflux, 68%, (c) Ph-B(OH)<sub>2</sub> or p-OMe-Ph-B(OH)<sub>2</sub>, Pd(PPh<sub>3</sub>)<sub>4</sub> or Pd(dppf)Cl<sub>2</sub>, NaHCO<sub>3</sub>, DME, H<sub>2</sub>O, heating, 41-94%, (d) conc. HCl, MeOH, 80°C, (e) Bn-Br, K<sub>2</sub>CO<sub>3</sub>, DMF, microwave heating, 85%, (f) R-I or R-Br, K<sub>2</sub>CO<sub>3</sub>, DMF, microwave heating, 20-65%. (g) Hydrazin or MeNH<sub>2</sub>.

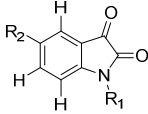
O=C1C(=O)N(R1)c2cc(R2)c(R3)c(R4)c(R5)c21

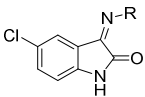
<sup>a</sup> The compounds displayed less than 90% but more than 50% inhibition, and the concentration-inhibition curves were accordingly fitted to the value of 100% inhibition (3 mM GABA).

<sup>b</sup> The bottom plateaus of the fitted curves were less than the GABA maximal inhibition plateau (set to 100%) and consequently gave the following relative maximum inhibition levels (% inhibition  $\pm$  S.D.): **hGAT1: 13**,  $53 \pm 4$ ; **hBGT1: 5**,  $60 \pm 5$ ; **8**,  $69 \pm 2$ ; **13**,  $79 \pm 4$ ; **hGAT2: 5**,  $60 \pm 8$ ; **8**,  $61 \pm 7$ ; **13**,  $72 \pm 8$ ; **hGAT3: 8**,  $87 \pm 5$ .

<sup>c</sup> The compound displayed less than 50% inhibition, and the IC<sub>50</sub> value was accordingly estimated as being greater than the highest tested concentration.

**Table 2.** Structure-activity relationships of isatin analogues at the four human GAT subtypes. Compounds were tested for their ability to inhibit uptake of 30 nM [<sup>3</sup>H]GABA at the four human GAT subtypes stably expressed in CHO cells. IC<sub>50</sub> values were determined by curve-fitting analysis and are based on at least three independent experiments, whereas compounds with no activity are based on at least two independent experiments. All data points were carried out in triplicates.

IC <sub>50</sub> (μM) (pIC <sub>50</sub> ± S.E.M)							
			hGAT1	hBGT1	hGAT2	hGAT3	GAT3/1 selectivity ratio
							
cmpd	R <sub>1</sub>	R <sub>2</sub>					
15	H	Et	532 <sup>a</sup> (3.27±0.01)	680 <sup>a</sup> (3.17±0.03)	643 <sup>a</sup> (3.20±0.06)	49 (4.34±0.12)	11
16	H	Sec-Bu	233 <sup>a</sup> (3.67±0.13)	100 (4.01±0.08)	171 (3.77±0.03)	15 (4.84±0.10)	16
17	H	Ph	876 <sup>b</sup> (3.07±0.07)	314 <sup>c</sup> (3.64±0.27)	63 <sup>c</sup> (4.24±0.13)	8 (5.09±0.09)	110
18	H	4-OMe-Ph	>1000	>1000 <sup>b</sup>	N.A.	>1000 <sup>b</sup>	-
19	H	3-thienyl	>1000	33 <sup>c</sup> (4.48±0.003)	50 <sup>c</sup> (4.32±0.02)	17 <sup>c</sup> (4.79±0.11)	>59
20	H	2-thienyl	>1000	749 <sup>c</sup> (3.21±0.19)	203 <sup>c</sup> (3.74±0.14)	6 <sup>c</sup> (5.20±0.05)	>167
21	H	<i>p</i> -toluyl	>1000	>1000 <sup>b</sup>	N.A.	22 <sup>c</sup> (4.66±0.05)	>45
22	H	<i>m</i> -toluyl	>1000	55 <sup>c</sup> (4.26±0.003)	63 <sup>c</sup> (4.20±0.002)	35 <sup>c</sup> (4.47±0.08)	>29
23	H	<i>o</i> -toluyl	>1000	50 <sup>c</sup> (4.30±0.02)	52 <sup>c</sup> (4.29±0.02)	24 <sup>c</sup> (4.63±0.09)	>42
24	H	2,6-OMe-Ph	N.T.	N.T.	N.T.	>300 <sup>b</sup>	-
25	H	(2,3-di-hydrobenzo [ <i>b</i> ][1,4]-dioxin-6-yl	N.T.	N.T.	N.T.	>300 <sup>b</sup>	-
26	H	( <i>E</i> )- styrenyl	N.T.	N.T.	N.T.	>300 <sup>b</sup>	-
27	H	naphtalen-1-yl	N.T.	N.T.	N.T.	>300 <sup>b</sup>	-

<b>28</b>	H	4-morpholino-phenyl	N.T.	N.T.	N.T.	>300 <sup>b</sup>	-
<b>29</b>	Me	Cl	906 <sup>a</sup> (3.04±0.03)	533 <sup>a</sup> (3.28±0.04)	421 <sup>a</sup> (3.39±0.07)	232 <sup>a</sup> (3.67±0.11)	3.9
<b>30</b>	Et	Cl	563 <sup>a</sup> (3.25±0.01)	453 <sup>a</sup> (3.35±0.05)	453 <sup>a</sup> (3.35±0.05)	124 (3.96±0.15)	4.5
<b>31</b>	nPr	Cl	248 <sup>a</sup> (3.61±0.03)	198 (3.71±0.04)	198 (3.71±0.04)	52 (4.31±0.12)	4.8
<b>32</b>	iPr	Cl	464 <sup>a</sup> (3.34±0.04)	235 <sup>a</sup> (3.63±0.02)	235 <sup>a</sup> (3.63±0.02)	46 (4.40±0.16)	10
<b>33</b>	nBu	Cl	184 (3.74±0.04)	140 (3.86±0.05)	140 (3.86±0.05)	53 (4.28±0.05)	3.5
<b>34</b>	Bn	Cl	>1000	>1000	>1000	29 <sup>c</sup> (4.65±0.18)	>34
<b>35</b>	4-MeBn	Cl	N.T.	N.T.	N.T.	>1000 <sup>b</sup>	-
<b>36</b>	3-MeBn	Cl	N.T.	N.T.	N.T.	>300 <sup>b</sup>	-
<b>37</b>	Naphtalen-2-ylmethyl	Cl	N.T.	N.T.	N.T.	>300 <sup>b</sup>	-
<b>38</b>	3-phenoxy-benzyl	Cl	N.T.	N.T.	N.T.	>300 <sup>b</sup>	-
<b>39</b>	Bn	<i>p</i> -toluyl	N.T.	N.T.	N.T.	>1000 <sup>b</sup>	-
<b>45</b>		R=Me	N.T.	N.T.	N.T.	>1000 <sup>b</sup>	-
<b>46</b>		R=NH <sub>2</sub>	N.T.	N.T.	N.T.	>1000 <sup>b</sup>	-

N.T. not tested

<sup>a</sup> The compounds displayed less than 90% but more than 50% inhibition, and the concentration-inhibition curves were accordingly fitted to the value of 100% inhibition (3 mM GABA).

<sup>b</sup> The compounds displayed less than 50% inhibition, and the IC<sub>50</sub> values were accordingly estimated as being greater than the highest tested concentration.

<sup>c</sup> The bottom plateaus of these fitted curves were less than the GABA maximal inhibition plateau (set to 100%) and consequently gave the following relative maximum inhibition levels (% inhibition ± std. dev.): **hBGT1**: compound **17**, 62 ± 9; compound **19**, 50 ± 11; 36 ± 14; compound **22**, 63 ± 9; compound **23**, 61 ± 6; **hGAT2**: compound **17**, 78 ± 7; compound **19**, 47 ± 21; compound **20**, 66 ± 7; compound **22**, 58 ± 17; compound **23**, 52 ± 14; **hGAT3**: compound **19**, 80 ± 10; compound **20**, 90 ± 2; compound **21**, 73 ± 1; compound **22**, 81 ± 8; compound **23**, 83 ± 8; compound **34**, 43 ± 11.